Biomaterials 71 (2015) 119–131

Contents lists available at ScienceDirect

Biomaterials

journal homepage: www.elsevier.com/locate/biomaterials

A microfluidically perfused three dimensional human liver model

Knut Rennert [a, 1], Sandra Steinborn [a, 1], Marko Gröger [a, i], Birgit Ungerböck [b], Anne-Marie Jank [c], Josef Ehgartner [d], Sandor Nietzsche [e], Julia Dinger [f], Michael Kiehntopf [g], Harald Funke [c], Frank T. Peters [f], Amelie Lupp [h], Claudia Gärtner [b], Torsten Mayr [d], Michael Bauer [i, j], Otmar Huber [a, j], Alexander S. Mosig [a, j, *]

[a] Institute of Biochemistry II, Jena University Hospital, 07743 Jena, Germany
[b] Microfluidic ChipShop GmbH, Stockholmer Straße 20, 07747 Jena, Germany
[c] Molecular Hemostaseology, Jena University Hospital, Jena, 07743 Jena, Germany
[d] Institute of Analytical Chemistry and Food Chemistry, Graz University of Technology, Graz, Austria
[e] Center for Electron Microscopy, Jena University Hospital, 07743 Jena, Germany
[f] Institute of Forensic Medicine, University Hospital Jena, 07743 Jena, Germany
[g] Department of Clinical Chemistry and Laboratory Medicine, Jena University Hospital, 07743 Jena, Germany
[h] Department of Pharmacology and Toxicology, Jena University Hospital, 07747 Jena, Germany
[i] Clinic of Anesthesiology and Intensive Care, Jena University Hospital, 07747 Jena, Germany
[j] Center for Sepsis Control and Care, Jena University Hospital, 07747 Jena, Germany

ARTICLE INFO

Article history:
Received 10 July 2015
Received in revised form
17 August 2015
Accepted 19 August 2015
Available online 25 August 2015

Keywords:
Liver
Organoid
Microfluidic biochip
Dynamic cell culture
Oxygen

ABSTRACT

Within the liver, non-parenchymal cells (NPCs) are critically involved in the regulation of hepatocyte polarization and maintenance of metabolic function. We here report the establishment of a liver organoid that integrates NPCs in a vascular layer composed of endothelial cells and tissue macrophages and a hepatic layer comprising stellate cells co-cultured with hepatocytes. The three-dimensional liver organoid is embedded in a microfluidically perfused biochip that enables sufficient nutrition supply and resembles morphological aspects of the human liver sinusoid. It utilizes a suspended membrane as a cell substrate mimicking the space of Disse. Luminescence-based sensor spots were integrated into the chip to allow online measurement of cellular oxygen consumption. Application of microfluidic flow induces defined expression of ZO-1, transferrin, ASGPR-1 along with an increased expression of MRP-2 transporter protein within the liver organoids. Moreover, perfusion was accompanied by an increased hepatobiliary secretion of 5(6)-carboxy-2′,7′-dichlorofluorescein and an enhanced formation of hepatocyte microvilli. From this we conclude that the perfused liver organoid shares relevant morphological and functional characteristics with the human liver and represents a new *in vitro* research tool to study human hepatocellular physiology at the cellular level under conditions close to the physiological situation.

1. Introduction

The liver plays a central role in metabolism, biotransformation of endogenous and exogenous substrates, and detoxification of xenobiotica. Non-parenchymal cells (NPCs) are essential for the physiological function of the liver. NPCs including Kupffer cells, stellate cells and endothelial cells account for about 40% of total liver cells. *Ex vivo* it has been shown that the presence of NPCs is a requirement for hepatocyte function [1]. Kupffer cells are specialized tissue macrophages that represent 15% of total liver cells and almost 80–90% of all tissue macrophages in the body [2]. Macrophages are key regulators of inflammatory response during infection and the major source of inflammatory cytokines such as interleukin (IL)-6 driving acute phase protein production in hepatocytes [3,4]. However, macrophages as well as hepatic stellate cells (HSCs) also mediate tissue regeneration in response to drug-induced liver damage [5], regulate the complex balance of inflammation and tissue regeneration [6,7], and facilitate cell–cell

* Corresponding author. Institute of Biochemistry II, Jena University Hospital, Nonnenplan 2-4 07743 Jena, Germany.
E-mail address: alexander.mosig@med.uni-jena.de (A.S. Mosig).
[1] These authors contributed equally to this publication.

http://dx.doi.org/10.1016/j.biomaterials.2015.08.043
0142-9612/

communication between hepatocytes and endothelial cells (ECs) [8]. HSCs and ECs represent 6% and 19% of total liver cells, respectively [9]. ECs do not simply form a barrier to restrict access of blood-borne compounds to the parenchyma, but also mediate clearance of i.e. endotoxins and bacteria, and regulate migration of leukocytes into the liver. The integrity of the liver microvasculature is thus fundamental for maintaining liver perfusion and cell viability [10].

In vitro monolayer cultures of hepatocytes are well-established in research but are accompanied by a reduction of major hepatic functions such as secretion of plasma proteins or detoxification due to down-regulation of several phase-I, -II and phase-III enzymes [11–13]. Co-culture approaches with NPCs have been shown to prevent hepatocyte dedifferentiation. Hepatocytes show improved urea production and a stable up-regulation of CYP1B1, CYP2C9, CYP2E1, and CYP3A4 during long-term co-culture with ECs [14–16]. Similarly, co-culture of hepatocytes and HSCs was reported to increase albumin secretion and CYP2B1/2 expression [17]. In addition to simple co-culture, three-dimensional liver tissue culture involving NPCs in contact with hepatocytes is required for improved maintenance of hepatocyte function [18,19]. In two-dimensional hepatocyte cultures a loss of hepatocyte cell polarization is frequently observed and associated with a diminished expression of distinct transporter proteins at the sinusoidal, basolateral and canalicular membranes [20].

So far, no *in vitro* model of the human liver is available that integrates ECs, macrophages and HSCs in co-culture with hepatocytes and also mimics the specific three-dimensional morphology of the human liver sinusoid, including the endothelial cell layer. While cells in the body are embedded and oriented in a complex three-dimensional network, *in vitro* tissue models need optimized perfusion strategies for a continuous supply of oxygen and nutrients. In addition, the removal of waste products is critical for culture of complex three-dimensional tissues with a high cellular density as diffusion of endogenous catabolites within tissues is impeded in static conditions. We recently introduced the Multi-Organ-Tissue-Flow (MOTiF) biochip design that features a suspended and freely perfusable membrane acting as a cell culture substrate [21]. Here, we report the establishment of a three-dimensional liver organoid embedded in microfluidically-supported biochips, which is structurally inspired by the morphology of the liver. HepaRG cells were used for the assembly of the liver organoids since preparation of primary liver cells is time- and cost-consuming. Moreover, availability of primary liver tissue specimens is often limited to donors suffering from pre-existing liver disorders and receiving extended medication. This likely affects liver cell function and contributes to experimental bias. To overcome these limitations, we used freshly isolated human umbilical vein endothelial cells (HUVEC) instead of liver sinusoidal endothelial cells (LSEC), since LSEC rapidly tend to de-differentiate *in vitro*, which is associated with a loss of fenestrae and re-organization of the cytoskeleton [22]. This de-differentiation process is difficult to monitor or control, and potentially adds an additional bias in day-to-day experimentation. Monocyte-derived macrophages were used to mimic Kupffer cell function and the immortalized human stellate cell line LX-2 as primary stellate cell surrogate. Immortalized cell lines have the advantage of continuous growth, unlimited availability and their clonal origin usually guarantees a constant phenotype allowing reproducible experimentation [23,24]. During culture in the biochip HepaRG cells consistently differentiate into cells exhibiting a hepatocyte phenotype and into cells with biliary epithelial cell phenotype that self-organize into a hepatocyte layer with functional bile ducts between hepatocyte-like cells [25] essential for liver function [26].

2. Material & methods

2.1. Cell culture

HepaRG: HepaRG cells were obtained from Biopredic International (Rennes, France). They were seeded at a density of 2.7×10^4 cells/cm^2 and cultured in William's Medium E (Biochrom, Berlin, Germany) containing 10% (v/v) FCS (Life Technologies, Darmstadt, Germany), 5 μg/ml insulin (Sigma–Aldrich, Steinheim, Germany), 2 mM glutamine (GIBCO, Darmstadt, Germany), 50 mM hydrocortisone-hemisuccinate (Sigma-Aldrich) and 100 U/ml Penicillin/100 μg/ml Streptomycin mixture (Pen/Strep) (GIBCO). The cells were cultured in a humidified cell incubator at 5% CO_2 and 37 °C for 14 days before differentiation. Medium was renewed every 3–4 days. Cell differentiation was induced as described [27] and cells were used up to 4 weeks. Endothelial cells: Human umbilical cord vein endothelial cells (HUVECs) were isolated from human umbilical cord veins as described [28]. Donors were informed about the aim of the study and gave written consent. HUVEC cells were seeded at a density of 2.5×10^4 cells/cm^2 and cultured in Endothelial Cell Medium (ECM) (Promocell, Heidelberg, Germany) up to passage 4. LX-2 stellate cells (kindly provided by Scott L. Friedman, Division of Liver Diseases, Mount Sinai School of Medicine, New York City, NY, USA) were seeded at a density of 2.0×10^4 cells/cm^2 and cultured in Dulbecco's Minimum Essential Medium (DMEM) (Biochrom) supplemented with 10% (v/v) FCS, 1 mM sodium pyruvate (GIBCO) and Pen/Strep. Peripheral Blood Mononuclear Cells (PBMCs) were isolated by Ficoll density gradient centrifugation as described previously [29] and seeded at a density of 1.0×10^6 cells/cm^2 in X-VIVO 15 medium (Lonza, Cologne, Germany) supplemented with 10% (v/v) autologous human serum, 10 ng/ml human granulocyte macrophage colony-stimulating factor (GM-CSF) (PeproTech, Hamburg, Germany) and Pen/Strep. After 3 h incubation in a humidified cell incubator at 5% CO_2 and 37 °C the cells were washed twice with X-VIVO 15 medium. Adherent monocytes were cultivated for 24 h in X-VIVO 15 medium and seeded into the liver organoid.

2.2. Liver organoid assembly

Liver organoids were assembled by staggered seeding of vascular and hepatic cell layers. In each sterilized biochip 2.7×10^5 HUVEC's/cm^2 (in total 3.0×10^5 cells) and 0.9×10^5/cm^2 monocytes (in total 1×10^5 cells) were mixed and seeded on top of the membrane in the upper chamber. HUVEC/monocytes were co-cultured for at least 5 days with a daily medium exchange in endothelial cell culture medium (ECM) supplemented with 10 ng/ml epidermal growth factor, 90 μg/ml heparin, 2.8 μM hydrocortisone, endothelial cell growth supplement, 10 ng/ml GM-CSF to induce macrophage differentiation, 100 U/ml penicillin/100 μg/ml streptomycin and 10% (v/v) autologous human serum (Life Technologies, Karlsruhe, Germany). M-CSF was not supplemented to the medium as human serum contains sufficient amounts for the differentiation of the macrophages [30–33]. Subsequently, 2.7×10^5/cm^2 differentiated HepaRG (in total 3×10^5 cells) and 3.6×10^5/cm^2 LX-2 (in total 4×10^4 cells) were seeded on the membrane at the opposite side of HUVEC cells and cultured for 24 h in DMSO-free William's Medium E (Biochrom, Berlin, Germany) hepatocyte growth medium containing 50 μM hydrocortisone, 10% (v/v) FBS containing, 5 μg/ml insulin, 2 mM glutamine and 100 U/ml penicillin/100 μg/ml streptomycin prior to experimental use.

2.3. Biochips

MOTiF biochips were made from cyclic olefin copolymers (COC) – TOPAS® and obtained from microfluidic ChipShop GmbH (Jena,

Germany). Biochips were manufactured as described previously [21]. Briefly, chips were made by injection molding. A 12.2 μm thick PET membrane (TRAKETCH) with a pore diameter of 8 μm and a pore density of 1×10^5 pores/cm^2 (Sabeu, Radeberg, Germany) was integrated. Chips and channel structures were sealed on top and bottom side with an extruded 140 μm thick COC foil using a low-temperature proprietary bonding method. Gas permeable silicon tubing was used for perfusion allowing oxygen equilibration during experiments. Ramping structures to avoid step transitions between membrane edges and channel structures have been introduced into the chip bulk to prevent unfavorable flow conditions and trapping of stationary bubbles. Stirring the cell culture medium and equilibration under perfusion conditions overnight reduced bubble formation within the chip. Further, oxygen plasma treatment for hydrophilization of the whole chip surface was performed to reduce in-chip air bubble formation. Details on dimensions of biochip structures and applied flow rates with corresponding shear stress rates (calculated for cell culture media used) are given in Supplementary Table 1.

2.4. Oxygen sensors

Oxygen sensors were applied via spray coating at the inlet and outlet of each chamber, allowing online detection of oxygen consumption of cultivated cells. These sensors are based on dynamic quenching principle of luminescence by molecular oxygen and allow contactless measurements of oxygen via frame positioned polymer fibers. Read-out and data acquisition were accomplished by a commercially available oxygen meter (Firesting, Pyroscience, Aachen, Germany). Characterization of COC for oxygen rediffusion was performed in a hypoxia incubator. Briefly, after equilibrating the gas- and medium-filled chamber of a biochip overnight at 0.5% oxygen level, rediffusion of oxygen into the locked chip at normoxic conditions was recorded. Where indicated, experiments at normoxic conditions were performed in a standard cell culture incubator. Oxygen consumption of static cultured cells in a locked COC-biochip was recorded over a time period of at least 16 h. Treatment of cells with 20 μM staurosporine (Sigma-Aldrich, Germany) was introduced as an assay control to induce cell death in the cells, resulting in loss of oxygen consumption and later in oxygen rediffusion into the biochip. Dynamic cultivation of the HepaRG cells was performed using a syringe pump (neMESYS, cetoni GmbH, Korbuβen, Germany) at the indicated flow rates.

2.5. Immunofluorescence microscopy, CDF-DA assay and ADP/ATP assay

Cells were fixed for 10 min with 4% paraformaldehyde at room temperature (RT). Staining was done with antibodies against: CYP3A4 (Merck-Millipore, Schwalbach, Germany), CD68 and ASGPR1 (BD Biosciences/Pharmingen, Heidelberg, Germany), ZO-1 (Life Technologies/Molecular Probes, Karlsruhe, Germany), MRP-2 (Cell Signaling Technology, Frankfurt, Germany), GFAP and Transferrin (Dako, Hamburg, Germany), and secondary antibodies goat-anti-rabbit-AF488, goat-anti-mouse-AF555 (Life Technologies/Molecular Probes), goat-anti-mouse-Cy3 and goat anti-rabbit Cy5 (Dianova, Hamburg, Germany), and DAPI (Life Technologies). Samples were embedded into fluorescent mounting medium (Dako). Image analyses and quantification of mean fluorescence intensities were performed by random field analyses with ImageJ2 software. MRP-2 activity was analyzed by incubation of HepaRG cell layers in serum-free Williams E medium (GIBCO) containing 5 μM 5(6)-Carboxy-2′,7′-dichlorofluorescein diacetate (CDFDA) (Sigma-Aldrich) at 37 °C for 15 min. Imaging was performed on an Axio Observer Z1 fluorescence microscope with ApoTome.2 equipment (Carl Zeiss AG, Jena, Germany). Images were analyzed using ImageJ2 software (Fiji). For measurement of cellular ADP and ATP content of HepaRG and LX-2 cells they were cultured at the bottom sealing foil of the biochip. For ADP/ATP measurement, the foil with attached cells was carefully cut out and adhesive cells treated with Nucleotide Releasing Buffer (abcam Cambridge, UK). Cells of the vascular layer were cultured at the membrane as described. ADP/ATP content and ratio was analyzed with the ADP/ATP Ratio Assay Kit (abcam) according to manufacturers instructions.

2.6. Analysis of CYP3A4 metabolite formation

Liver organoids were cultured for 72 h in absence or presence of LPS, respectively. Medium was exchanged every 24 h. Subsequently, liver organoids were incubated for 6 h with serum-free hepatocyte culture medium containing Midazolam (Rotexmedica, Trittau, Germany), provided as an aqueous solution at 13.8 mM (5 mg/ml) and diluted to a final concentration of 3 μM. After protein precipitation and concentration, samples were analyzed using an LC-MS/MS system consisting of an ABSciex QTrap 4000 tandem mass spectrometer (Darmstadt, Germany) equipped with a Turbo V ion spray source and coupled to an LC-20 liquid chromatography system (Shimadzu, Jena, Germany). Separation was performed on a ZORBAX Eclipse XDBC18 column (4.6 × 150 mm, 5 μm) from Agilent (Böblingen, Germany) using a gradient program with 50 mM ammonium formiate buffer plus 0.75% (v/v) formic acid (eluent A) and acetonitrile (eluent B). The mass spectrometer was operated in scheduled multiple reaction monitoring (MRM) mode using the target transition *m/z* 342 to 324 for quantification of 1-OH-midazolam. Instrument control, data acquisition, and data evaluation were performed using Analyst software 1.6.2 (ABSciex, Darmstadt, Germany).

2.7. Scanning electron microscopy

Cells were fixed with 2.5% (v/v) glutaraldehyde in cacodylate buffer for 120 min. Afterwards the samples were washed thrice with cacodylate buffer for 10 min and dehydrated in ascending ethanol concentrations (30, 50, 70, 90 and 100%) for 10 min each. Subsequently, the samples were critical-point dried using liquid CO_2 and sputter coated with gold (thickness approx. 4 nm) using a SCD005 sputter coater (BAL-TEC, Liechtenstein) to avoid surface charging. Finally the specimens were investigated with a field emission (FE) SEM LEO-1530 Gemini (Carl Zeiss NTS GmbH, Oberkochen, Germany).

Lactate, Glucose, Albumin, Urea, ASAT, ALAT, GLDH and LDH measurements.

The respective parameters were measured in cell culture supernatants using the Abbott Architect ci8200 Integrated System (Abbott Laboratories, Abbott Park, IL, USA) according to the manufacturer's protocol.

2.8. Statistics

All results are reported as average of the performed experiments with standard deviation. Where indicated, statistics were done with two-tailed, non-paired Student's t-test or One-way ANOVA with Tukey's multiple comparison test. Statistical analysis was performed using GraphPad Prism 6.07 software (Graphpad Software, La Jolla, CA, USA).

3. Results

A human liver sinusoid is formed by the sinusoidal wall composed of endothelial cells interspersed with immune-

modulatory monocyte-derived macrophages. This vascular layer is separated from the underlying hepatic tissue of hepatocytes and stellate cells by the space of Disse (Fig. 1). We adapted this morphological structure in our human liver model by assembling a vascular and a hepatic cell layer grown on the opposite sides of a suspended micro-porous membrane. The membrane serves as a substrate for both cell layers thereby separating them from each other and concomitantly mimicking the space of Disse (Fig. 1).

The vascular cell layer is composed of HUVECs which are co-cultured with differentiated primary monocyte-derived macrophages at the apical side of the suspended membrane. On the opposite side of the membrane, the hepatic cell layer is formed by differentiated HepaRG hepatocyte-like cells, which are co-cultured with LX-2 stellate cells. This setting facilitates stabilization of the multilayered three-dimensional tissue and allows intercellular cross-communication of co-cultured cell layers through the 12 μm thick membrane containing pores of 8 μm diameter (Fig. 2A). As shown in Fig. 2 B and C, artificial tissue sheets in the biochip showed structural similarities to primary precision cut liver tissue slices with a similar density and distribution of macrophages and stellate cells, respectively. Primary stellate cells in liver slices were stained for glial fibrillary acidic protein (GFAP), a well-established marker protein for non-activated stellate cells [34].

Prolonged culture of human primary hepatocytes is associated with a significant loss of expression of phase-I cytochrome P450 enzymes [35,36]. Therefore, we tested whether co-culture with endothelial cells in the biochip improves growth and morphology of HepaRG and CYP expression. Under these conditions CYP3A4 expression was clearly increased in HepaRG cells. Furthermore, no adverse effects on CYP3A4 expression levels by co-culturing macrophages or stellate cells in this setup were observed (Fig. 2D, E).

Oxygen saturation of the cell culture medium is a critical parameter for the regulation of the metabolic capacity of hepatocytes. To perform contactless, real-time in-chip measurements of oxygen levels during cell culture luminescence-based sensor spots were integrated into the biochips at the inlets and outlets of both perfusion channels [37] (Fig. 3 A, B). To individually characterize oxygen uptake of cell layers, we measured the time-dependent decline of oxygen saturation in the upper vascular (via sensor spots 1 and 2; Fig. 3 A, B) as wells as the HepaRG compartment (via sensor spots 3 and 4; Fig. 3 A, B) during static cell culture. A significant decline of oxygen saturation within approximately 16 h down to 47% of the maximal oxygen saturation within the culture medium (max. O_2 sat.) was observed in the vascular compartment containing HUVEC cell layers, and a nearly complete oxygen depletion down to 4% max. O_2 sat. in the HepaRG compartment. A similar oxygen decline was observed after replacing of the medium by fresh, air equilibrated cell culture medium. After more than 37 h of static culture we found a comparable kinetic of oxygen consumption in the culture medium indicating that cell layers within the biochip are unaffected, still viable and metabolic active (Fig. 3C, D). To verify that the decline of oxygen levels within the biochip depends on the metabolic activity of cultured cells, apoptosis was induced by treatment with staurosporine [38] (Fig. 3C, D). After a short initial phase of oxygen depletion, the oxygen consumption subsequently decreased in response to death of the embedded cells and passive oxygen re-diffusion through the chip bulk material. The oxygen resupply by diffusion throughout the biochip bulk material was slightly slower than diffusion rates observed in control experiments without cultured cells (Supplementary Figure 1), indicating some remaining cell viability after staurosporine treatment.

Next, we wanted to determine the impact of different perfusion rates on oxygen consumption by HepaRG cells, calculated as the difference between oxygen saturation at the inlet and outlet of the chamber (Δ oxygen saturation). For the first 200 min the co-culture was perfused with 1 μl/min at both cell layers. A significant drop of oxygen levels at the inlet of the perfusion channel, which however was significantly lower than under static culture conditions was detectable. This indicates that oxygen consumption through HepaRG cells is faster than oxygen re-supply through media perfusion at 1 μl/min (Fig. 3 E). Increasing the perfusion rate up to 3 μl/min resulted in a stable oxygen level at the inlet of the HepaRG cell chamber of around 95% max. O_2 saturation. Analysis of the difference in oxygen saturation at the inlet and outlet of the channel system allowed to estimate the metabolic activity of the HepaRG cell layer. Interestingly, HepaRG oxygen consumption was elevated in response to increased perfusion rate (Fig. 3 F).

Moreover, we addressed the impact of medium perfusion under normoxic and hypoxic conditions on cellular energy levels by measurement of intracellular ATP and ADP contents of HepaRG cells. ATP levels were found significantly decreased under hypoxic conditions in static as well as perfused cultures of the liver organoids (Fig. 4 A). Intracellular ADP levels seemed unaffected by medium perfusion under normoxic conditions, but slightly declined in the dynamic culture of organoids under hypoxic conditions. In order to determine the cell fate, intracellular ADP/ATP ratio was calculated (Fig. 4 B). A low ADP/ATP ratio based on the high ATP and low ADP levels was assumed to correlate with a

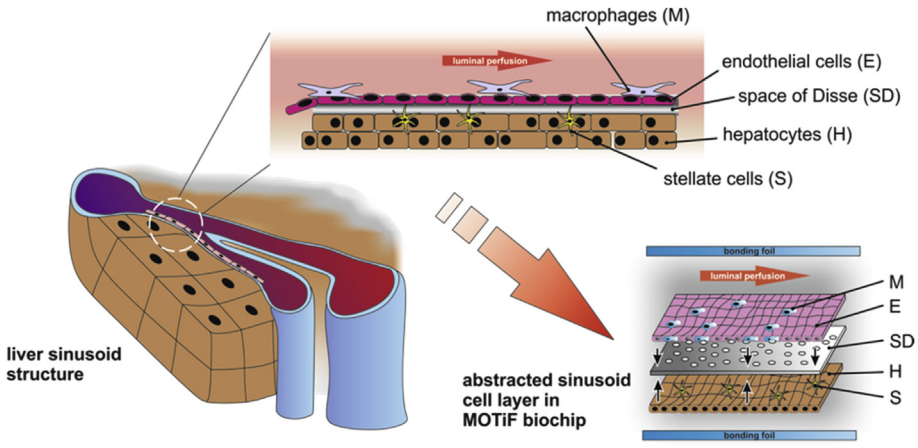

Fig. 1. Adaption of the *in vivo* morphology of the human liver sinusoid in a multi-layered liver organoid. The three-dimensional liver organoid consists of a vascular layer formed by endothelial cells (E) and primary macrophages (M), and a hepatic layer comprising hepatocyte-like HepaRG cells (H) co-cultured with stellate cells (S). The space of Disse (SD) is mimicked by the biochip-embedded membrane serving as a scaffold allowing cell–cell communication through its pores.

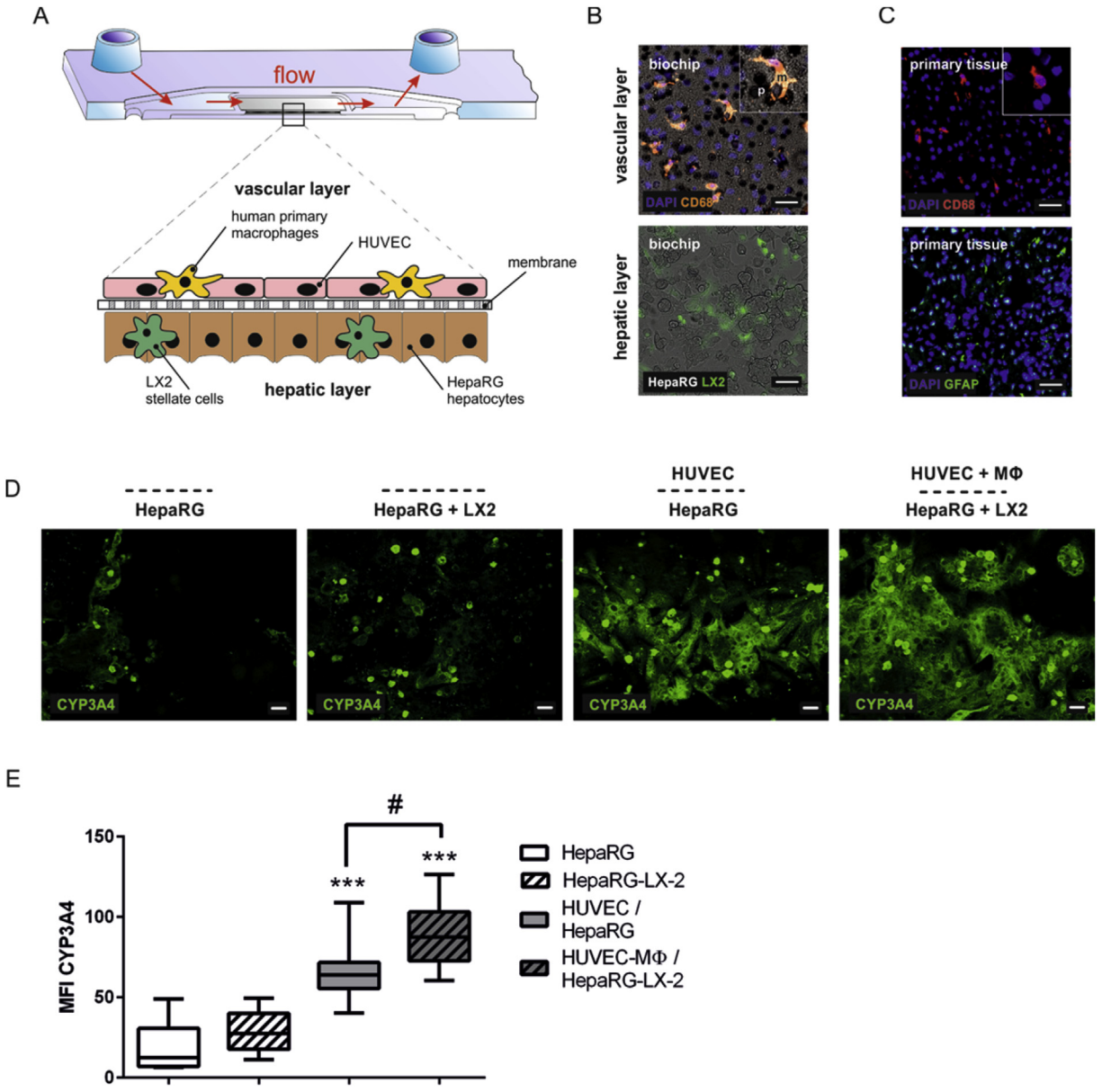

Fig. 2. Establishment of a three-dimensional liver model in a microfluidic biochip. A) Cross-section of the biochip-embedded liver model. B) Immunostaining of macrophages (CD68, orange) and nuclei (DAPI, blue) of cells of the vascular layer. Bright field microscopic image of the HepaRG layer. For visualization purposes LX-2 stellate cells were labeled with CellTracker Green CMFDA dye immediately before seeding the cells. Liver organoids were cultured for 4 days. C) Immunostaining of macrophages (CD68, red) and primary stellate cells (GFAP, green) in primary liver tissue. B–C) scale bar 50 μm; D) Effect of NPC co-culture on CYP3A4 protein expression (green) in HepaRG cells. The black bar above the microscopic image represents the chip membrane and localization of individual cell types relative to the membrane is noted. Scale bar 50 μm. E) Quantification of CYP3A4 mean fluorescence intensity (MFI) in regions of interest (ROI) of three independent experiments. Significance was calculated using One-Way-ANOVA with Tukey's multiple comparison test (***$p < 0.01$ vs. HepaRG mono-culture, #$p < 0.05$ between indicated conditions). D-E) Liver organoids were cultured for 4 days. (For interpretation of the references to color in this figure legend, the reader is referred to the web version of this article.)

proliferative state of cells cultured under normoxic conditions, irrespective of medium perfusion. Under hypoxic conditions however, the ADP/ATP ratio was significantly increased under static but not dynamic conditions. As the cellular ATP content in static, hypoxic culture was also lower than the ADP level, this is indicative for cell death under these conditions. In dynamic, hypoxic cultures, ATP levels were found increased relative to ADP levels resulting in a low ADP/ATP ratio pointing to a growth arrest (Supplementary Table 2).

An appropriate polarization of hepatocytes is a prerequisite for the formation of functionally active hepatic bile canaliculi and represents an important characteristic of the HepaRG cell line. To address this point, the expression and localization of various hepatic differentiation and polarization marker proteins including the differentiation marker proteins asialoglycoprotein receptor-1 (ASGPR-1), zonula occludens-1 (ZO-1) and multidrug resistance-associated protein-2 (MRP-2) was analyzed. ASGPR-1 is a transmembrane protein that is specifically expressed in the liver at the sinusoidal and basolateral hepatocellular membranes, but not on the bile canalicular (also called apical) membrane [39–41]. ZO-1, which is located at the tight junctions (TJs) marks the margins of the bile canaliculi [42], and the multidrug resistance-associated protein-2 (MRP-2), a major hepatic transporter protein, defines the apical membrane of polarized hepatocytes [43]. Normal ASGPR-

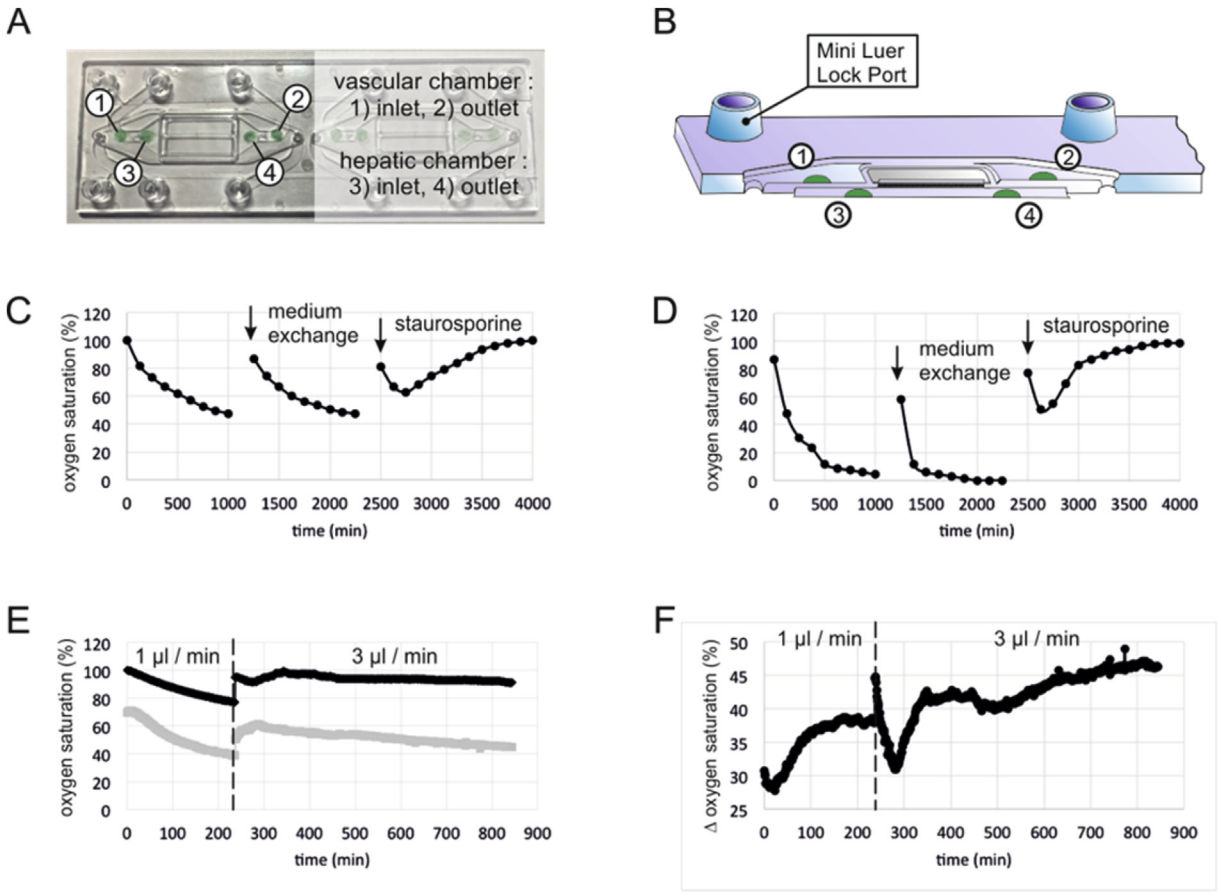

Fig. 3. Measurement of oxygen saturation in cell culture medium by fluorescence emitting sensor spots. A) Integration of oxygen sensor spots in the microfluidically supported biochip. Sensor spots were integrated at the inlets (1, 3) and the outlets (2, 4) of the upper and lower channel systems, respectively. B) Schematic cross-section of the biochip with integrated oxygen sensor spots. C, D) Oxygen saturation of the medium measured at the outlets of the upper vascular compartment containing HUVECs (C), and the lower compartment containing hepatocyte-like HepaRG cells (D). Both cell layers were co-cultured within the MOTiF biochips. The time point of medium exchange with fresh, air-equilibrated medium and exchange for fresh, air-equilibrated medium containing 20 μM staurosporine are indicated by arrows above the graph lines. E) Measurement of oxygen consumption of HepaRG cell layer co-cultured with an HUVEC cell layer at the membrane under microfluidic flow. Oxygen saturation was measured at the inlet (black line) and the outlet (gray line) of the HepaRG biochip compartment. F) Calculated oxygen consumption of perfused HepaRG cell layers calculated from the difference between oxygen saturation at the inlet and outlet of HepaRG biochip compartment. E–F) Oxygen saturation was initially measured at a cell perfusion rate of 1 μl/min and was subsequently increased to 3 μl/min (right to the dashed line). C–F) Oxygen saturation measurements were performed with cell layers pre-cultured for 24 h within the biochip.

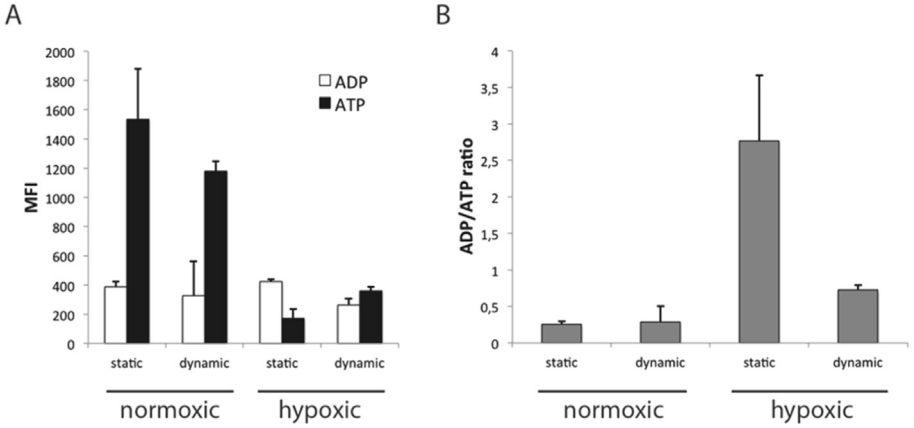

Fig. 4. Cellular ADP and ATP content of HepaRG cell layers co-cultured with HUVEC cell layer on the opposite sides of the membrane within MOTiF biochips for 4 days under static and dynamic culture conditions. A) Cellular ADP (open bars) and ATP (black bars) levels in cells cultured under normal oxygen levels (21% O_2) and under hypoxic conditions (5% O_2) for 72 h. B) ADP/ATP ratios measured with luciferase assays. Mean fluorescence intensity (MFI) represents cellular ATP and ADP content.

1 expression and distribution was observed within HepaRG monocultures. However, the compact co-culture of stellate cells, endothelial cells or/and macrophages under static conditions resulted in a loss of defined ASGPR-1 protein expression and a delocalization of the protein from the basolateral membrane (Fig. 5 A). Also ZO-1 was diminished and delocalized in HepaRG when co-cultured with NPCs under static conditions (Fig. 5 B). MRP-2 expression was found highly expressed in monolayer cultures of HepaRG, and its expression pattern was lost in static co-cultures of HepaRG and NPCs (Fig. 5 C). In agreement with this finding the activity of MRP-2, as assayed by release of the fluorescent dye 5-(and 6)-carboxy-2′,7′-dichlorofluorescein (CDF) into bile canaliculi-like structures of HepaRG [44] was decreased. In consequence, the CDF dye was trapped within the cytoplasm of HepaRG cells resulting in unfocused staining (Fig. 5 D).

In the human liver a shear stress at the sinusoidal endothelium of 10–50 mPa has been reported [45]. However, the direct shear stresses experienced by hepatocytes is difficult to estimate as the effects of flow are dampened by the separation of hepatocytes from sinusoidal blood by liver sinusoidal ECs and the space of Disse [10]. It even appears that hepatocytes are sensitive to the application of shear stress and that only extremely low shear stress is tolerated [46]. We observed increased oxygen consumption of HepaRG cells in response to elevated cell perfusion with increased shear forces that might induce cellular stress. To avoid this stress effect and to prevent potential cell damage the liver organoids were perfused in

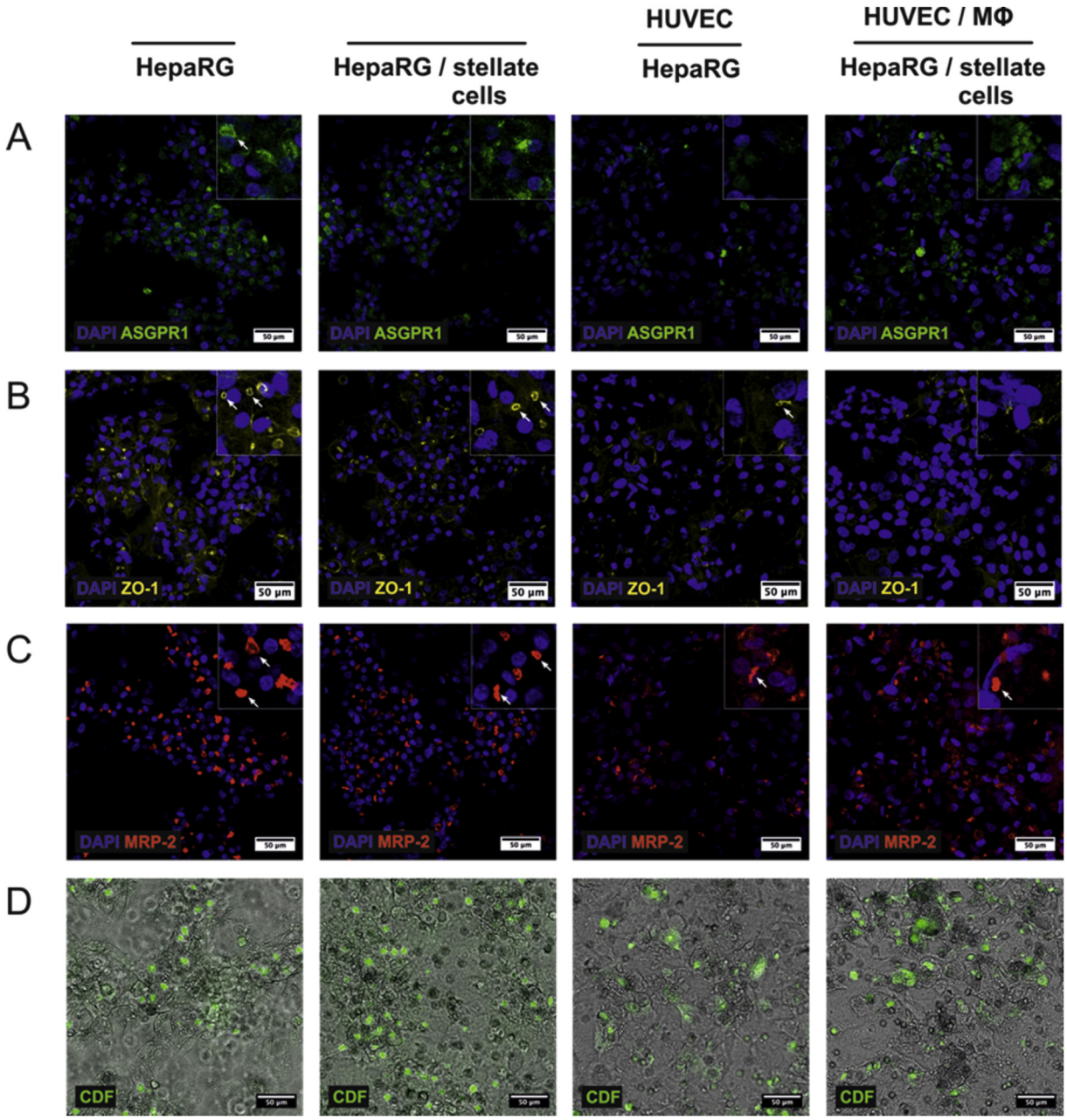

Fig. 5. Immunostaining of specific markers in the HepaRG cell layer during step-wise assembly of the liver organoids. A) ASGPR-1 (green), B) ZO-1 (yellow), C) MRP-2 (red). A-C) Cell nuclei (DAPI, blue). D) Assessment of MRP-2 activity in HepaRG cells by measurement of CDF-release (green) into bile canaliculi-like structures. Scale bar 20 µm. The line above the images represents the chip-embedded membrane and indicates localization of each individual cell type relative to the membrane. A-D) Cell layers were cultured for 4 days within biochips. (For interpretation of the references to color in this figure legend, the reader is referred to the web version of this article.)

a more physiological way only at the vascular side ("vascular perfusion") resembling the *in vivo* situation with a shear stress rate of 50 mPa·(0.5 dyn/cm^2), which equals a perfusion rate of 50 μl/min in the MOTiF biochip. Vascular perfusion for 96 h resulted in the formation of a highly confluent EC layer with an increased expression of VE-cadherin at endothelial cell–cell contacts revealing similarities with the VE-cadherin expression pattern observed in primary human precision cut liver slices (Fig. 6 A). Thus dynamic perfusion significantly improves the polarization of ECs in the vascular layer of the liver organoids.

In static co-cultures of HepaRG and LX-2 cell clusters are surrounded by cells with a biliary epithelial phenotype. In contrast, the vascular perfusion induced the formation of a confluent homogenous HepaRG cell layer without cluster formation (Fig. 6 B). Moreover, the HepaRG cell layers in perfused liver organoids displayed an increased and stable expression of CYP3A4 (Fig. 6 B, 7 A) that was associated with elevated metabolization of midazolam as detected by the formation of its metabolite 1-hydroxy-midazolam (1-OH-midazolam) after 6 h incubation. In addition, perfused organoids exhibited a defined and stable pattern of ASGPR-1 expression that highly correlated with the morphology and expression pattern observed in primary human liver tissue (Fig. 6 C). Compared to static cultures, transferrin expression was also markedly increased in perfused liver organoids with expression levels close to the levels detectable in primary liver tissue slices (Fig. 6 D). Furthermore, perfused liver organoids revealed a ZO-1 staining along elongated structures correlating with an enhanced formation of bile canaliculi-like structures between HepaRG cells (Fig. 6 E). MRP-2 expression (Fig. 6 F) and function was also significantly increased in perfused liver organoids as detected by CDF excretion assays displaying a focused release of CDF into self-organized bile canaliculi-like structures not observable under static conditions (Fig. 7 C).

MRP-2 is located along the microvilli of hepatocytes [47]. When perfused liver organoids were compared with static tissue culture by scanning electron microscopy. HepaRG cells exhibited an increased plasticity with a higher density of microvilli compared to static tissue culture that showed a flattened cell structure with significantly reduced numbers of microvilli (Fig. 8 A). This finding correlated well with the defined expression pattern of ZO-1 and MRP-2 (Fig. 6 B) and the enhanced CDF secretion in perfused liver organoids (Fig. 7 A). In addition to the enhanced MRP-2 secretory capacity, perfused liver organoids also exhibited significantly enhanced synthesis of albumin and urea, compared to statically cultured liver organoids or conventional monolayer cultures of hepatocytes (Fig. 8 B–C).

Next we addressed the cellular oxygen consumption in the whole liver organoid during vascular perfusion. In contrast to static culture, where a fast drop of oxygen saturation was observed, vascular perfusion with 50 μl/min was sufficient for stable oxygen supply to the vascular cell layer of the liver organoid (Fig. 8 D). Similarly, in the HepaRG compartment of the lower biochip chamber a rapid oxygen consumption was detectable under static cell culture conditions. However, in contrast to the vascular cell layer a medium perfusion only temporally increased oxygen saturation at the chamber inlet that declined within 8 h to a virtually complete oxygen exhaustion within the HepaRG chamber (Fig. 8 E). In this context we were interested whether the adaption of HepaRG cells to hypoxia is reversible. Therefore, we measured oxygen consumption of HepaRG cells as surrogate of their metabolic activity under static conditions as well as direct perfusion conditions. After complete oxygen exhaustion within the HepaRG compartment we initiated perfusion of the HepaRG layer by a stepwise increase in perfusion rates. At a perfusion rate of 1 μl/min, oxygen levels still declined with time at the channel inlet, and dissolved oxygen was entirely consumed during media flow through the organoid. Applying a perfusion rate of 3 μl/min, oxygen supply at the channel inlet was constant. However, after an initial increase, oxygen levels at the chamber outlet still declined over time (Fig. 8 F). An increase of the flow rate up to 10 μl/min resulted in stable oxygen levels at the inlet and outlet of the chamber. Highest difference of oxygen saturation at the inlet and outlet of the chamber was measured at a perfusion rate of 3 μl/min (Fig. 8 G).

Taken together, oxygen consumption correlated with increasing perfusion rates. During cell culture the air pressure was 760 mmHg and oxygen solubility in the cell culture medium was estimated k = 1.19 nmol/ml/mmHg [48,49]. Under these conditions we calculate mean oxygen saturation difference as $\Delta_{\text{saturation}}$

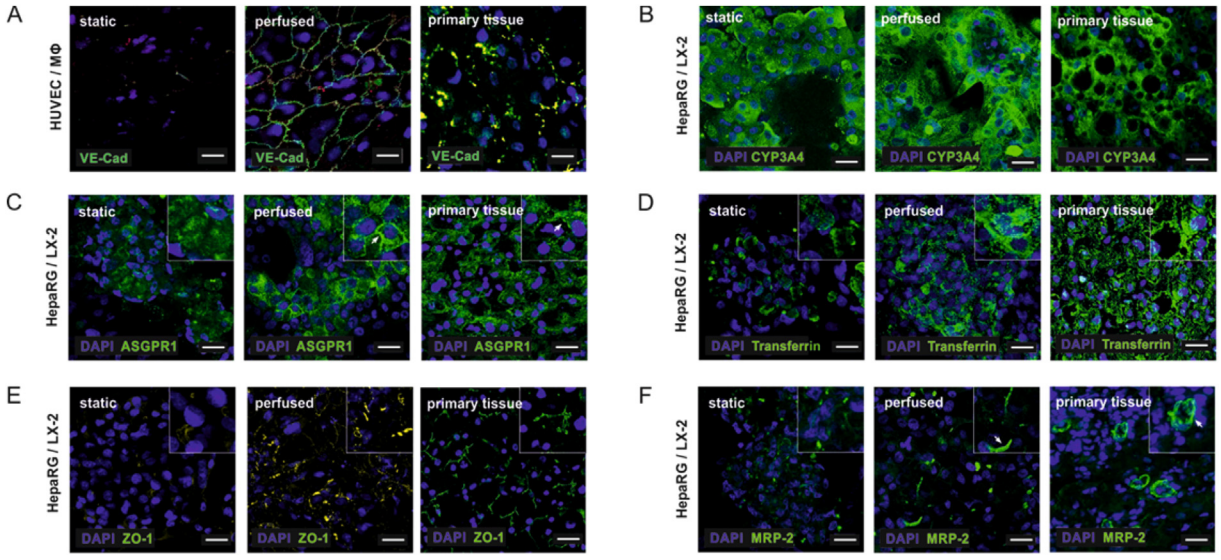

Fig. 6. Immunostaining of liver organoids cultured under static and perfused conditions. Perfused liver organoid share morphological similarities with primary human precision cut liver tissue (primary tissue). A) VE-cadherin (green) expression and localization within the vascular layer of the organoid. Cell nuclei (DAPI, blue) (scale bar 20 μm). B–F) Immune staining of B) CYP3A4 (green), C) ASGPR-1 (green), D) transferrin (green), E) ZO-1 (yellow) and F) MRP-2 (green). B–F) Cell nuclei (DAPI, blue). Scale bar 50 μm. A-F) Liver organoids were cultured for 4 days under indicated conditions. (For interpretation of the references to color in this figure legend, the reader is referred to the web version of this article.)

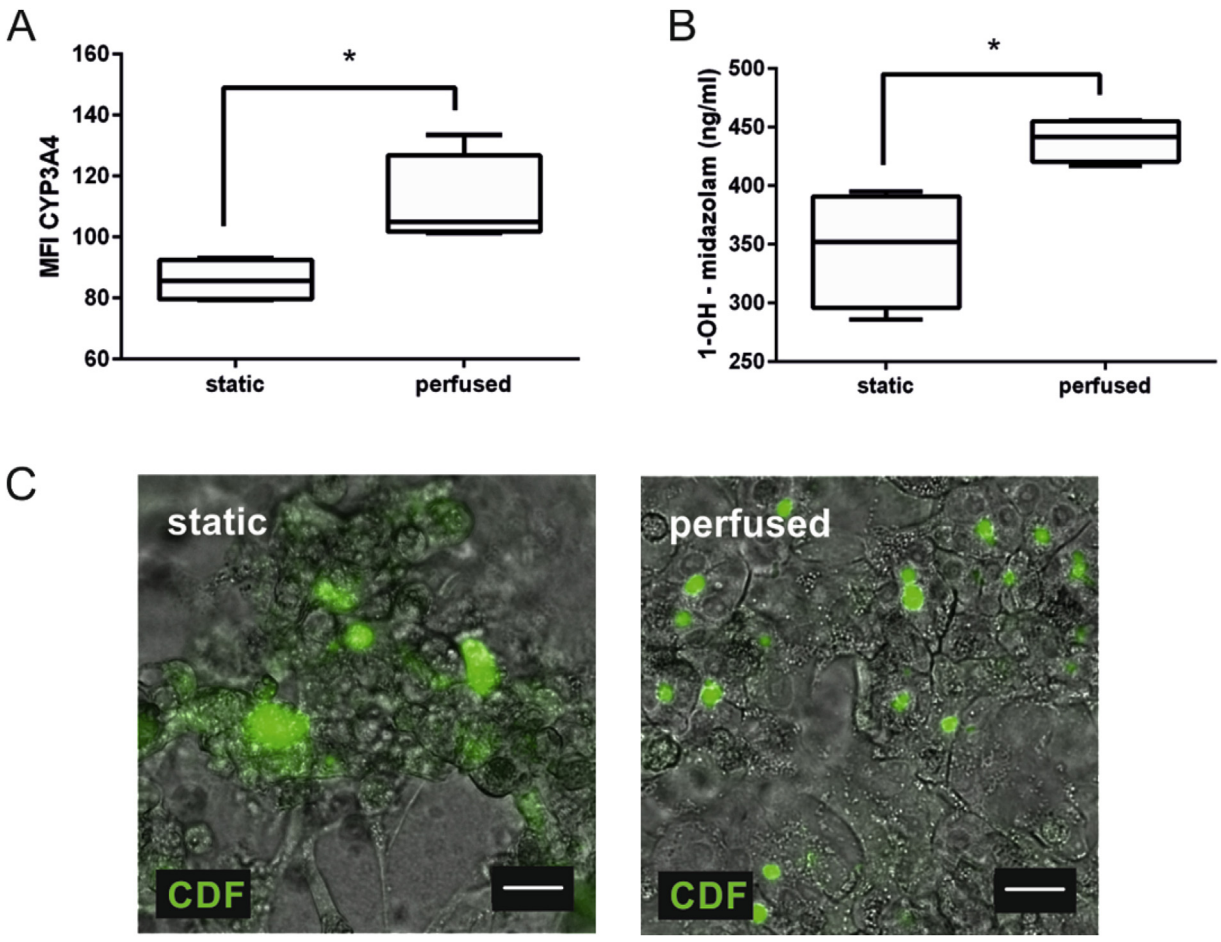

Fig. 7. Comparison of metabolic activities in the liver organoid under static and dynamic culture conditions. A) Analysis of CYP3A4 expression by immunofluorescence image analysis. B) Formation of the metabolite 1-OH-midazolam by CYP3A4 A-B) Significance was calculated using Student's t-test (*p < 0.05) C) Assessment of MRP-2 activity in hepatocytes of organoids cultured under static or perfused conditions by measurement of CDF-release (green) into bile canaliculi-like structures (scale bar 20 μm). A-C) Liver organoids were cultured for 4 days under static or perfused conditions. (For interpretation of the references to color in this figure legend, the reader is referred to the web version of this article.)

$_{\text{level}} = O_2\ sat\cdot_{\ inlet} - O_2\ sat\cdot_{\ outlet}$, where O_2 *sat.* is the mean oxygen saturation level measured at the inlet and outlet of the chamber, respectively. Oxygen consumption is then calculated $O_2\ con\cdot = (k{*}0,209{*}760\ mmHg){*}(O_2\ sat\cdot_{\ inlet} - O_2\ sat\cdot_{\ outlet}){*}flow\ rate$, where O_2 *sat.* is the mean oxygen saturation level measured at the inlet and outlet of the chamber, respectively. Our results indicate that increasing liver organoid perfusion rates correlate with elevated cellular oxygen consumption likely due to improved nutrient supply and associated higher metabolic activity under well-perfused culture conditions (Table 1).

4. Discussion

Most studies addressing liver physiology or organ dysfunction were performed using animal models of mice and rats. However, a controversial debate about the usefulness of rodent models and the transferability of the obtained data to human conditions was raised [50,51]. *In vitro* organoid models of the liver facilitate studies with human liver tissue and prevent potential bias due to interspecies differences and thus offer an attractive alternative to animal models. *In vitro* models can be used under reproducible and standardized conditions and are reasonably cost effective, whereas animal models need extensive service and maintenance to ensure i.e. sufficient environmental control for reliable experimentation [52,53].

In vitro hepatocyte monolayers are a frequently used tool. However, under static conditions in conventional cell culture dishes, unfavorable high media-to-cell volume ratios exist. Recently, it was shown that decreasing media-to-cell volume ratios resulted in the formation of higher concentrations of drug metabolites [54]. Cell culture of 3×10^5 HepaRG/LX-2 cells in MOTiF biochips requires only 120 μl of culture medium (0.4 nl/hepatocyte) making it a suitable tool for substance screening on a micro-scale basis with minimized wastage of test compounds. The low media-to-cell ratio in our biochip-based assays increases the resulting medium concentrations of metabolites and thereby facilitates application of assays to measure metabolites.

A close interaction between endothelial cells and hepatocytes is required to maintain normal morphology and sufficient CYP enzyme expression [16,55]. These stabilizing effects of ECs on the expression as well as the activity of CYP3A4 in HepaRG cells are mediated through the pores of the scaffold membrane in our biochip model. Layer-wise assembling strategies were also applied by other groups. When rat hepatocytes and bovine aortic endothelial cells were co-cultured on opposing sides of a transwell filter, hepatocytes remained differentiated and secreted urea [55]. Similar results were obtained in a model of stacked cell layers of rat hepatocytes and bovine carotid artery endothelial cells [56]. However, these models do not allow investigations under humanized

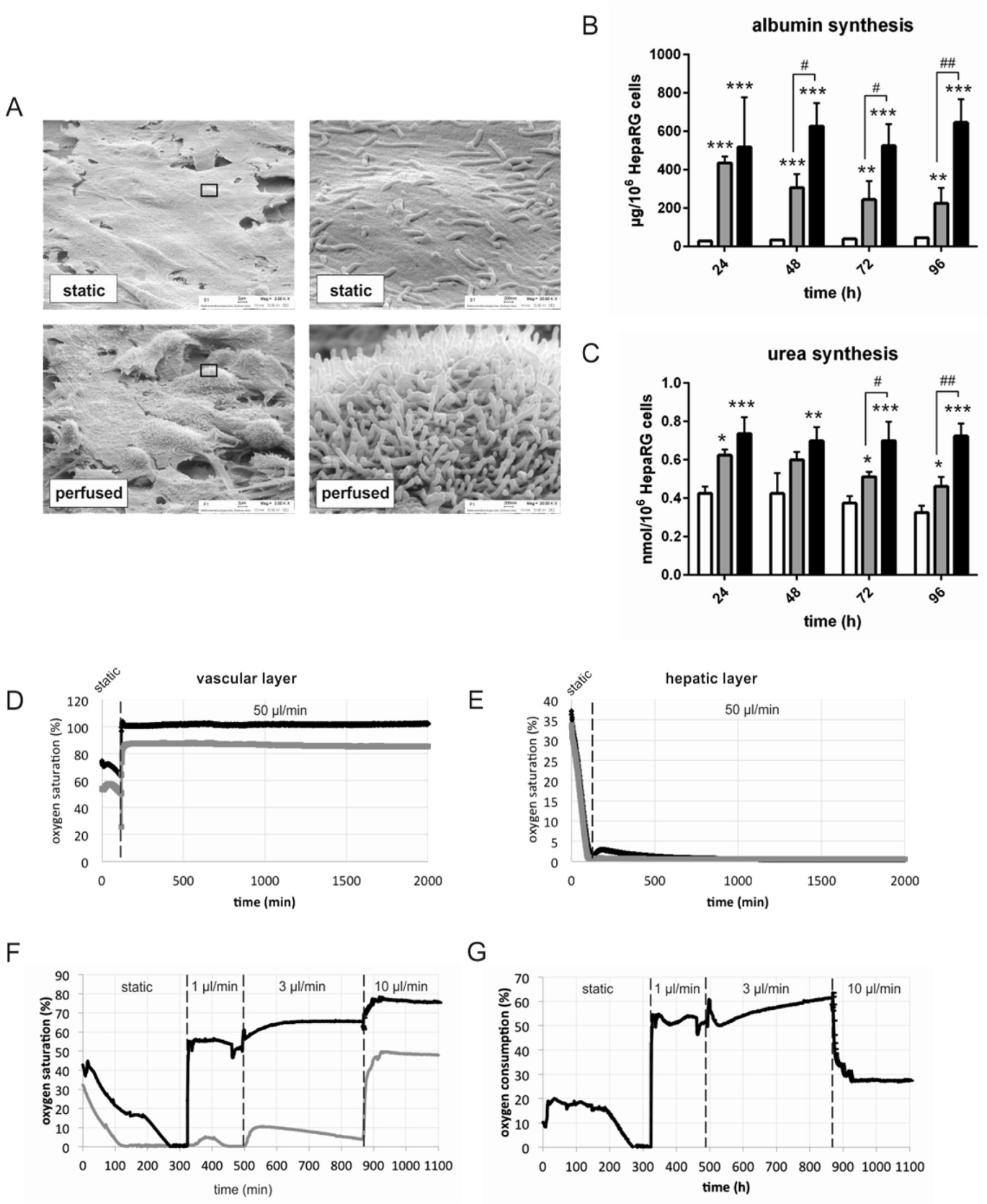

Fig. 8. Comparison of microstructure and oxygen consumption of liver organoids under static and dynamic culture conditions. A) Scanning electron microscopic images of HepaRG cells in the liver organoids cultured under static or perfused culture conditions. Rectangle in left side images marks magnified area of images shown at the right side. HepaRG cells under perfusion revealed higher cell plasticity with increased microvilli formation at the cell surface (scale bar 2 µm left side, 200 nm right side). Release of B) albumin and C) urea by monocultures of HepaRG cells under static conditions in a cell culture dish (open bars) and organoids cultured within MOTiF biochips under static (gray bars) and dynamic

Table 1
Oxygen consumption of liver organoids under flow conditions.

Perfusion rate	Mean $\Delta_{inlet/outlet}$ Saturation level (%)	Total O_2 consumption (nmol/min/10^6 cells)
1 μl/min	51.91	0.3271
3 μl/min	56.50	1.0680
10 μl/min	29.30	1.8461

conditions. Other studies have shown that extracellular matrix (ECM) proteins such as collagen, fibronectin and laminin produced by endothelial cells promote hepatocyte differentiation [56] and preserve hepatocyte morphology concomitant with a stable secretion of albumin and urea, and an elevated hepatocyte drug metabolizing ability [57,58]. Moreover, hepatocyte growth factor (HGF), which is produced by LSEC and also HUVEC, was reported to mediate long-term survival and polarization of hepatocytes in co-culture with HUVEC [56,59–61]. We suppose that similar effects contribute to HepaRG phenotype preservation in our liver model. Larkin et al. reported a more complex model of rat LSEC and Kupffer cells separated by a chitosan-hyaluronic acid polymer layer from collagen embedded primary rat hepatocytes. Under static culture conditions the hepatocytes maintained their phenotype without signs of dedifferentiation [62]. A biodegradable chitosan membrane was also used by Salerno et al. for co-culture of human primary hepatocytes with HUVEC, where beneficial effects of the co-culture on hepatocyte albumin production, urea synthesis and drug biotransformation again was reported [63]. All these observations underline the importance of NPCs on maintenance of hepatocellular function.

An important step forward to further optimize culture conditions in our liver organoid model was the application of microfluidic flow mimicking *in vivo* vascular perfusion. The more complex and highly packed cell layers formed on the membrane within the biochip apparently consume more oxygen and produce considerably more waste products in limited volumes of available cell culture medium. Thus, the perfusion of the multilayered organoids is advantageous for efficient supply with oxygen and removal of waste products, to stabilize the morphology, polarization and excretory function of HepaRG cells. Other perfused *in vitro* liver models have been previously reported. Toh et al. utilized micropillars mimicking fenestrated ECs that act as a shield to protect hepatocytes during perfusion with culture medium [64]. However, due to the absence of NPCs and the lack of essential cell–cell contacts or paracrine signals this model does not really reflect the physiological regulation of hepatocellular function and polarization. Cell–cell communication between ECs and hepatocytes under perfusion was established in a model published by Domansky et al., in which flow-mediated simulation of physiological shear stress conditions allowed to maintain viability and phenotype of hepatocytes up to 13 days [65]. Recently, Esch et al. reported the establishment of a three-dimensional model of the human liver, consisting of defined ratios of hepatocytes and non-parenchymal cells (fibroblasts, stellate cells, and Kupffer cells) [66]. Fluidic flow of medium was emulated by placing the chip on a rocking platform. In this simplified perfusion approach, an increase of albumin and urea synthesis of co-cultured hepatocytes was achieved. However, an organized *in vivo*-like morphology including an endothelial cell layer covering hepatocytes is missing.

A striking feature of the liver is the difference of metabolic activity of hepatocytes depending on oxygen gradient along the liver acinus [67]. *In-chip* oxygen measurement under flow conditions by luminescence emitting sensor spots not only represents a valuable tool for assessment of cellular activity of assembled liver organoids but can also be used as a surrogate of HepaRG metabolic activity. Our measurements indicate that in our biochip under vascular perfusion conditions an oxygen gradient mimicking *in vivo* conditions is formed as a consequence of enhanced oxygen consumption and prevention of free oxygen diffusion from the upper chamber throughout the organoid.

The oxygen gradient formed by vascular perfusion likely restricts uncontrolled cell growth, contributes to the maintenance of the cellular architecture of the organoid and is adaptable by simple adjustment of the perfusion rate. Hepatocytes quickly depolarize upon loss of cell–cell contacts in response to removal from native tissue complexes [68]. Repolarization during liver organoid formation is thus an important prerequisite for an effective excretory activity and the removal of xenobiotics and catabolites from the cells. The localization of ASGPR-1, ZO-1 and MRP-2 confirms functional polarization of hepatocytes necessary for bile secretion and barrier formation [69]. Perfusion of the liver organoid further increased metabolic activity as detectable by enhanced urea and albumin synthesis, which was also reported by other multi-cellular liver models [66,70,71]. Moreover, we assume that the oxygen gradient formed by unilateral perfusion of the vascular layer contributes to the observed hepatocyte polarization. Our microfluidic biochip-based liver organoid thus holds the potential to mimic liver acinus zonation, enabling the development of *in vitro* platforms to study liver zonation [72]. Follow-up studies will be performed to examine this in detail.

Our experiments showed that under microfluidic perfusion HepaRG cells are able to dynamically adapt to normoxic as well as hypoxic conditions as revealed by changes in cellular ADP/ATP ratios. However, in case of static culture with restricted oxygen and nutrition supply together with enrichments of catabolites cellular damage is induced. *In vivo* similar conditions are observed in response to ischemia, which is also associated with cellular damage and organ dysfunction.

In conclusion, we here demonstrated the establishment of a functional liver organoid comprising all major liver cell types. The liver model displays clear differentiation and structural reorganization and enables polarization closely resembling primary human liver tissue *in vitro*. It is functionally stable for at least four days after full assembly and with perfusion. Studies are underway to characterize viability under long-term culture. The compact biochip in the size of a standardized microscope slide further facilitates *on-chip* tissue observation with conventional bright field or fluorescence microscopy [21,73] or spectrometric methods such as near infrared spectroscopy [74] enabling real-time analysis under flow conditions. We are convinced that this liver model is a valuable tool to study liver physiology, metabolism and the underlying molecular processes at the cellular level. It paves the way for detailed *in vitro* studies on the role of particular NPCs on hepatocellular function under physiological and pathophysiological conditions, i.e. in

culture conditions (filled bars) for up to 96 h. Students t-Test: compared to corresponding HepaRG monocell culture: *p < 0.05; **p < 0.01; ***p < 0.001; compared to indicated condition #p < 0.05; ##p < 0.01; E–H) Measurement of oxygen consumption of liver organoids under static and microfluidic flow. Oxygen saturation was measured at the inlet (black line) and the outlet (gray line) of the vascular and HepaRG biochip compartment at indicated perfusion rates. D–E) Oxygen saturation in at the vascular layer (D) and HepaRG layer (E) of the organoid during unilateral vascular perfusion. F-G) Perfusion of the HepaRG cell layer. Oxygen saturation was initially measured at static conditions and subsequently with cell perfusion rates of 1, 3 and 10 μl/min. The vascular layer was simultaneously perfused with 50 μl/ml. F) Oxygen consumption of the liver organoid measured in the HepaRG compartment. G) Calculated oxygen consumption of perfused organoid from the difference between oxygen saturation at the inlet and outlet of HepaRG biochip compartment. A–G) Liver Organoids were cultured for 4 days within biochips.

toxicological or pharmacological screening. The principal utility of biochip-based assays has already been proven for simple endothelial and HepaRG cell cultures in assays aimed to characterize functionalized nanoparticles as new therapeutic treatment options of liver disease [75]. Furthermore, the modular assembly of the liver model described in this study is ideally suited to address the role of specific genes or proteins in the cell types of interest for liver function. Cells with a knock-out/down of the gene of interest or overexpressing a mutated variant thereof can be easily integrated into the liver organoid for subsequent functional analyses. The integration of the organoid into a versatile, microfluidically supported platform with standardized microscopical slide dimensions allows real-time in-chip analyses with established analytical microscopic and/or spectrometric methods and state-of-the-art biosensor applications.

Author contributions

KR, SS, JD, MG, BU, AML, SN performed the experiments. JE, MK, TM, AL, HF, FP contributed reagents/materials/analysis tools. KR, SS, BU, SN, MG, ASM analyzed the data. KR, MB, AL wrote parts of the manuscript. OH, ASM wrote the manuscript. KR and ASM planned experiments. ASM designed and supervised the study.

Acknowledgments

We are grateful to the excellent technical work of Christina Ness, Maria Franke and Margot Voigt. We thank the team of the Placenta Laboratory of the Jena University Hospital for supplying umbilical cords for HUVEC isolation. The authors would further like to acknowledge support of this work by 2011 VF 0005 grant of the Thüringer Aufbaubank (Germany) and by the FK 1328-511 grant from the Federal Agency on Risk Assessment (Germany). This work was further supported by the Federal Ministry of Education and Research (Germany), FKZ: 01EO1002.

Appendix A. Supplementary data

Supplementary data related to this article can be found at http://dx.doi.org/10.1016/j.biomaterials.2015.08.043.

References

[1] D.M. Bissell, D.M. Arenson, J.J. Maher, F.J. Roll, Support of cultured hepatocytes by a laminin-rich gel. Evidence for a functionally significant subendothelial matrix in normal rat liver, J. Clin. Investig. 79 (1987) 801–812.
[2] L. Bouwens, M. Baekeland, R. De Zanger, E. Wisse, Quantitation, tissue distribution and proliferation kinetics of Kupffer cells in normal rat liver, Hepatology 6 (1986) 718–722.
[3] E. Seki, S. De Minicis, C.H. Osterreicher, J. Kluwe, Y. Osawa, D.A. Brenner, et al., TLR4 enhances TGF-beta signaling and hepatic fibrosis, Nat. Med. 13 (2007) 1324–1332.
[4] T.R. Billiar, R.D. Curran, D.L. Williams, P.H. Kispert, Liver nonparenchymal cells are stimulated to provide interleukin 6 for induction of the hepatic acute-phase response in endotoxemia but not in remote localized inflammation, Archives Surg. 127 (1992) 31–36 (discussion 6–7).
[5] M.P. Holt, L. Cheng, C. Ju, Identification and characterization of infiltrating macrophages in acetaminophen-induced liver injury, J. Leukoc. Biol. 84 (2008) 1410–1421.
[6] I.N. Crispe, The liver as a lymphoid organ, Annu. Rev. Immunol. 27 (2009) 147–163.
[7] C. Kordes, I. Sawitza, D. Haussinger, Hepatic and pancreatic stellate cells in focus, Biol. Chem. 390 (2009) 1003–1012.
[8] J. Kasuya, R. Sudo, T. Mitaka, M. Ikeda, K. Tanishita, Hepatic stellate cell-mediated three-dimensional hepatocyte and endothelial cell triculture model, Tissue Eng. Part A 17 (2011) 361–370.
[9] Z. Kmiec, Cooperation of liver cells in health and disease, Adv. Anat. Embryol. Cell Biol. 161 (2001). III-XIII, 1–151.
[10] E.L. LeCluyse, R.P. Witek, M.E. Andersen, M.J. Powers, Organotypic liver culture models: meeting current challenges in toxicity testing, Crit. Rev. Toxicol. 42 (2012) 501–548.
[11] D.F. Clayton, A.L. Harrelson, J.E. Darnell Jr., Dependence of liver-specific transcription on tissue organization, Mol. Cell Biol. 5 (1985) 2623–2632.
[12] J.Z. Tong, P. De Lagausie, V. Furlan, T. Cresteil, O. Bernard, F. Alvarez, Long-term culture of adult rat hepatocyte spheroids, Exp. Cell Res. 200 (1992) 326–332.
[13] P. Godoy, N.J. Hewitt, U. Albrecht, M.E. Andersen, N. Ansari, S. Bhattacharya, et al., Recent advances in 2D and 3D in vitro systems using primary hepatocytes, alternative hepatocyte sources and non-parenchymal liver cells and their use in investigating mechanisms of hepatotoxicity, cell signaling and ADME, Arch. Toxicol. 87 (2013) 1315–1530.
[14] J. Schutte, B. Hagmeyer, F. Holzner, M. Kubon, S. Werner, C. Freudigmann, et al., Artificial micro organs''–a microfluidic device for dielectrophoretic assembly of liver sinusoids, Biomed. Microdevices 13 (2011) 493–501.
[15] M. Ohno, K. Motojima, T. Okano, A. Taniguchi, Induction of drug-metabolizing enzymes by phenobarbital in layered co-culture of a human liver cell line and endothelial cells, Biol. Pharm. Bull. 32 (2009) 813–817.
[16] M. Ohno, K. Motojima, T. Okano, A. Taniguchi, Up-regulation of drug-metabolizing enzyme genes in layered co-culture of a human liver cell line and endothelial cells, Tissue Eng. Part A 14 (2008) 1861–1869.
[17] S.F. Abu-Absi, J.R. Friend, L.K. Hansen, W.S. Hu, Structural polarity and functional bile canaliculi in rat hepatocyte spheroids, Exp. Cell Res. 274 (2002) 56–67.
[18] J. Landry, D. Bernier, C. Ouellet, R. Goyette, N. Marceau, Spheroidal aggregate culture of rat liver cells: histotypic reorganization, biomatrix deposition, and maintenance of functional activities, J. Cell Biol. 101 (1985) 914–923.
[19] F.J. Wu, J.R. Friend, R.P. Remmel, F.B. Cerra, W.S. Hu, Enhanced cytochrome P450 IA1 activity of self-assembled rat hepatocyte spheroids, Cell Transpl. 8 (1999) 233–246.
[20] F. Berthiaume, P.V. Moghe, M. Toner, M.L. Yarmush, Effect of extracellular matrix topology on cell structure, function, and physiological responsiveness: hepatocytes cultured in a sandwich configuration, FASEB J. 10 (1996) 1471–1484.
[21] M. Raasch, K. Rennert, T. Jahn, S. Peters, T. Henkel, O. Huber, et al., Microfluidically supported biochip design for culture of endothelial cell layers with improved perfusion conditions, Biofabrication 7 (2015) 015013.
[22] A.J. Ford, G. Jain, P. Rajagopalan, Designing a fibrotic microenvironment to investigate changes in human liver sinusoidal endothelial cell function, Acta Biomater. 24 (2015) 220–227.
[23] R. Weiskirchen, J. Weimer, S.K. Meurer, A. Kron, B. Seipel, I. Vater, et al., Genetic characteristics of the human hepatic stellate cell line LX-2, PloS One 8 (2013) e75692.
[24] J. Herrmann, A.M. Gressner, R. Weiskirchen, Immortal hepatic stellate cell lines: useful tools to study hepatic stellate cell biology and function? J. Cell Mol. Med. 11 (2007) 704–722.
[25] V. Cerec, D. Glaise, D. Garnier, S. Morosan, B. Turlin, B. Drenou, et al., Transdifferentiation of hepatocyte-like cells from the human hepatoma HepaRG cell line through bipotent progenitor, Hepatology 45 (2007) 957–967.
[26] D.H. Adams, S.C. Afford, The role of cholangiocytes in the development of chronic inflammatory liver disease, Front. Biosci. 7 (2002) e276–85.
[27] P. Gripon, S. Rumin, S. Urban, J. Le Seyec, D. Glaise, I. Cannie, et al., Infection of a human hepatoma cell line by hepatitis B virus, Proc. Natl. Acad. Sci. U.S.A. 99 (2002) 15655–15660.
[28] M. Wallert, S. Mosig, K. Rennert, H. Funke, M. Ristow, R.M. Pellegrino, et al., Long-chain metabolites of α-tocopherol occur in human serum and inhibit macrophage foam cell formation in vitro, Free Radic. Biol. Med. (2014) 43–51.
[29] S. Mosig, K. Rennert, S. Krause, J. Kzhyshkowska, K. Neunübel, R. Heller, et al., Different functions of monocyte subsets in familial hypercholesterolemia: potential function of CD14+ CD16+ monocytes in detoxification of oxidized LDL, FASEB J Fed. Am. Soc. Exp. Biol. (2009) 866–874.
[30] K. Yong, N. Salooja, R.E. Donahue, U. Hegde, D.C. Linch, Human macrophage colony-stimulating factor levels are elevated in pregnancy and in immune thrombocytopenia, Blood 80 (1992) 2897–2902.
[31] J. Cebon, J.E. Layton, D. Maher, G. Morstyn, Endogenous haemopoietic growth factors in neutropenia and infection, Br. J. Haematol. 86 (1994) 265–274.
[32] K.M. Irvine, M.R. Andrews, M.A. Fernandez-Rojo, K. Schroder, C.J. Burns, S. Su, et al., Colony-stimulating factor-1 (CSF-1) delivers a proatherogenic signal to human macrophages, J. Leukoc. Biol. 85 (2009) 278–288.
[33] M. Naito, G. Hasegawa, Y. Ebe, T. Yamamoto, Differentiation and function of Kupffer cells, Med. Electron Microsc. 37 (2004) 16–28.
[34] R. Liao, H. Wu, Y. Yi, J.X. Wang, X.Y. Cai, H.W. He, et al., Clinical significance and gene expression study of human hepatic stellate cells in HBV related-hepatocellular carcinoma, J. Exp. Clin. Cancer Res. 32 (2013) 22.
[35] V.Y. Soldatow, E.L. Lecluyse, L.G. Griffith, I. Rusyn, models for liver toxicity testing, Toxicol. Res. Camb. 2 (2013) 23–39.
[36] G. Luo, T. Guenthner, L.S. Gan, W.G. Humphreys, CYP3A4 induction by xenobiotics: biochemistry, experimental methods and impact on drug discovery and development, Curr. Drug Metab. 5 (2004) 483–505.
[37] C. Gärtner, B. Ungerbröck, I. Schulz, T. Jahn, A. Mosig, T. Mayr, et al., Sensor enhanced microfluidic devices for cell based assays and organs on chip, in: Proceedings SPIE, Smart Biomedical and Physiological Sensor Technology XII, 2015.
[38] M. Andersson, J. Sjostrand, A. Petersen, A.K. Honarvar, J.O. Karlsson, Caspase and proteasome activity during staurosporin-induced apoptosis in lens epithelial cells, Invest. Ophthalmol. Vis. Sci. 41 (2000) 2623–2632.
[39] T. Terada, M. Iwai, S. Kawakami, F. Yamashita, M. Hashida, Novel PEG-matrix

metalloproteinase-2 cleavable peptide-lipid containing galactosylated liposomes for hepatocellular carcinoma-selective targeting, J. Control Release 111 (2006) 333–342.
[40] D.A. Wall, A.L. Hubbard, Galactose-specific recognition system of mammalian liver: receptor distribution on the hepatocyte cell surface, J. Cell Biol. 90 (1981) 687–696.
[41] M. Spiess, The asialoglycoprotein receptor: a model for endocytic transport receptors, Biochemistry 29 (1990) 10009–10018.
[42] J.M. Anderson, J.L. Glade, B.R. Stevenson, J.L. Boyer, M.S. Mooseker, Hepatic immunohistochemical localization of the tight junction protein ZO-1 in rat models of cholestasis, Am. J. Pathol. 134 (1989) 1055–1062.
[43] G. Jedlitschky, U. Hoffmann, H.K. Kroemer, Structure and function of the MRP2 (ABCC2) protein and its role in drug disposition, Expert Opin. Drug Metab. Toxicol. 2 (2006) 351–366.
[44] M.J. Zamek-Gliszczynski, H. Xiong, N.J. Patel, R.Z. Turncliff, G.M. Pollack, K.L. Brouwer, Pharmacokinetics of 5 (and 6)-carboxy-2′,7′-dichlorofluorescein and its diacetate promoiety in the liver, J. Pharmacol. Exp. Ther. 304 (2003) 801–809.
[45] P.F. Lalor, D.H. Adams, Adhesion of lymphocytes to hepatic endothelium, Mol. Pathol. 52 (1999) 214–219.
[46] H. Miyoshi, T. Ehashi, H. Kawai, N. Ohshima, S. Suzuki, Three-dimensional perfusion cultures of mouse and pig fetal liver cells in a packed-bed reactor: effect of medium flow rate on cell numbers and hepatic functions, J. Biotechnol. 148 (2010) 226–232.
[47] P. Recknagel, F.A. Gonnert, M. Westermann, S. Lambeck, A. Lupp, A. Rudiger, et al., Liver dysfunction and phosphatidylinositol-3-kinase signalling in early sepsis: experimental studies in rodent models of peritonitis, PLoS Med. 9 (2012) e1001338.
[48] M.L. Yarmush, M. Toner, J.C. Dunn, A. Rotem, A. Hubel, R.G. Tompkins, Hepatic tissue engineering. Development of critical technologies, Ann. N. Y. Acad. Sci. 665 (1992) 238–252.
[49] Y. Nahmias, Y. Kramvis, L. Barbe, M. Casali, F. Berthiaume, M.L. Yarmush, A novel formulation of oxygen-carrying matrix enhances liver-specific function of cultured hepatocytes, FASEB J. 20 (2006) 2531–2533.
[50] H.S. Warren, R.G. Tompkins, L.L. Moldawer, J. Seok, W. Xu, M.N. Mindrinos, et al., Mice are not men, Proc. Natl. Acad. Sci. U.S.A. 112 (2015) E345.
[51] J. Seok, H.S. Warren, A.G. Cuenca, M.N. Mindrinos, H.V. Baker, W. Xu, et al., Genomic responses in mouse models poorly mimic human inflammatory diseases, Proc. Natl. Acad. Sci. U.S.A. Natl. Acad. Sci. (2013) 3507–3512.
[52] M.H. Tschop, J.R. Speakman, J.R. Arch, J. Auwerx, J.C. Bruning, L. Chan, et al., A guide to analysis of mouse energy metabolism, Nat. Methods 9 (2012) 57–63.
[53] J. Nedergaard, B. Cannon, The browning of white adipose tissue: some burning issues, Cell Metab. 20 (2014) 396–407.
[54] S.S. Bale, G.V. Sridharan, I. Golberg, L. Prodanov, W.J. McCarty, O.B. Usta, et al., A novel low-volume two-chamber microfabricated platform for evaluating drug metabolism and toxicity, Technology 0 (2015) 1–8.
[55] Y.B. Kang, S. Rawat, J. Cirillo, M. Bouchard, H.M. Noh, Layered long-term co-culture of hepatocytes and endothelial cells on a transwell membrane: toward engineering the liver sinusoid, Biofabrication 5 (2013) 045008.
[56] K. Kim, K. Ohashi, R. Utoh, K. Kano, T. Okano, Preserved liver-specific functions of hepatocytes in 3D co-culture witsh endothelial cell sheets, Biomaterials 33 (2012) 1406–1413.
[57] J.C. Dunn, M.L. Yarmush, H.G. Koebe, R.G. Tompkins, Hepatocyte function and extracellular matrix geometry: long-term culture in a sandwich configuration, FASEB J. 3 (1989) 174–177.
[58] A. Bader, E. Knop, A. Kern, K. Boker, N. Fruhauf, O. Crome, et al., 3-D coculture of hepatic sinusoidal cells with primary hepatocytes-design of an organotypical model, Exp. Cell Res. 226 (1996) 223–233.
[59] Y. Toyoda, M. Tamai, K. Kashikura, S. Kobayashi, Y. Fujiyama, T. Soga, et al., Acetaminophen-induced hepatotoxicity in a liver tissue model consisting of primary hepatocytes assembling around an endothelial cell network, Drug Metabol. Dispos. Biol. Fate Chem. 40 (2012) 169–177.
[60] A. Soto-Gutierrez, N. Navarro-Alvarez, H. Yagi, Y. Nahmias, M.L. Yarmush, N. Kobayashi, Engineering of an hepatic organoid to develop liver assist devices, Cell Transpl. 19 (2010) 815–822.
[61] Y. Nahmias, R.E. Schwartz, W.S. Hu, C.M. Verfaillie, D.J. Odde, Endothelium-mediated hepatocyte recruitment in the establishment of liver-like tissue in vitro, Tissue Eng. 12 (2006) 1627–1638.
[62] A.L. Larkin, R.R. Rodrigues, T.M. Murali, P. Rajagopalan, Designing a multicellular organotypic 3D liver model with a detachable, nanoscale polymeric Space of Disse, Tissue Eng. Part C Methods 19 (2013) 875–884.
[63] S. Salerno, C. Campana, S. Morelli, E. Drioli, L. De Bartolo, Human hepatocytes and endothelial cells in organotypic membrane systems, Biomaterials 32 (2011) 8848–8859.
[64] Y.C. Toh, T.C. Lim, D. Tai, G. Xiao, D. van Noort, H. Yu, A microfluidic 3D hepatocyte chip for drug toxicity testing, Lab Chip 9 (2009) 2026–2035.
[65] K. Domansky, W. Inman, J. Serdy, A. Dash, M.H.M. Lim, L.G. Griffith, Perfused multiwell plate for 3D liver tissue engineering, Lab Chip (2010) 51.
[66] M.B. Esch, J.M. Prot, Y.I. Wang, P. Miller, J.R. Llamas-Vidales, B.A. Naughton, et al., Multi-cellular 3D human primary liver cell culture elevates metabolic activity under fluidic flow, Lab Chip 15 (2015) 2269–2277.
[67] T.D. Boyer, T.L. Wright, M.P. Manns, D. Zakim, Zakim and Boyer's Hepatology: a Textbook of Liver Disease, Saunders/Elsevier, Philadelphia, PA, 2006.
[68] G. Elaut, T. Henkens, P. Papeleu, S. Snykers, M. Vinken, T. Vanhaecke, et al., Molecular mechanisms underlying the dedifferentiation process of isolated hepatocytes and their cultures, Curr. Drug Metab. 7 (2006) 629–660.
[69] D. Fu, Y. Wakabayashi, Y. Ido, J. Lippincott-Schwartz, I.M. Arias, Regulation of bile canalicular network formation and maintenance by AMP-activated protein kinase and LKB1, J. Cell Sci. 123 (2010) 3294–3302.
[70] I. Wagner, E.M. Materne, S. Brincker, U. Sussbier, C. Fradrich, M. Busek, et al., A dynamic multi-organ-chip for long-term cultivation and substance testing proven by 3D human liver and skin tissue co-culture, Lab Chip 13 (2013) 3538–3547.
[71] S.S. Bale, I. Golberg, R. Jindal, W.J. McCarty, M. Luitje, M. Hegde, et al., Long-term coculture strategies for primary hepatocytes and liver sinusoidal endothelial cells, Tissue Eng. Part C Methods 21 (2015) 413–422.
[72] S.S. Bale, L. Vernetti, N. Senutovitch, R. Jindal, M. Hegde, A. Gough, et al., In vitro platforms for evaluating liver toxicity, Exp. Biol. Med. (Maywood) 239 (2014) 1180–1191.
[73] H. Becker, I. Schulz, A. Mosig, T. Jahn, C. Gärtner, Microfluidic devices for cell culture and handling in organ-on-a-chip applications, SPIE MOEMS-MEMS SPIE. 8976 (2014) 1–9.
[74] M. Lange, S. Engelhardt, S. Liebold, H. Plettenberg, S. Mosig, M. Hoffmann, Analysis of glucose and fetal calf serum in aqueous solution for Multi Organ Tissue Flow (MOTiF) bioreactors using NIR Spectroscopy, Biomed. Techn. Berl. 58 (2013) 4199.
[75] A.T. Press, A. Traeger, C. Pietsch, A. Mosig, M. Wagner, M.G. Clemens, et al., Cell type-specific delivery of short interfering RNAs by dye-functionalised theranostic nanoparticles, Nat. Commun. (2014) 5565.